UNIVERSITY OF AMSTERDAM

REPORT

Modeling Infectious Diseases

Student:
Kimon Anagnostopoulos
Student ID: 12345678

Lecturer: Valeria Krzhizhanovskaya

Course:
Introduction to Computational Science

September 22, 2025

Contents

Abstract

A numerical investigation of the susceptible-infectious-recovered (SIR) model and related epidemiological variants was performed using Python-based simulations. Parameter sweeps confirmed the threshold phenomenon at the basic reproduction number $R_0 = \beta/\gamma = 1$. Calibration to the 1978 British boarding school influenza outbreak produced transmission and recovery rates of $\beta = 1.665$ day^{-1} and $\gamma = 0.448$ day^{-1}, respectively, resulting in $R_0 = 3.72$ and a critical vaccination threshold of 73.1 percent. Analysis of vaccination strategies indicated that preventative coverage above the herd immunity threshold prevents epidemics, while emergency mass vaccination at rates exceeding 100 individuals per day substantially reduces peak prevalence. Incorporating demographic processes with birth and death rates $\mu = 1/70$ year^{-1} resulted in endemic equilibria characterized by 2.4-year oscillation periods. The susceptible-exposed-infectious-recovered (SEIR) variant exhibited delayed epidemic peaks due to latent periods. Introducing seasonal forcing, defined as $\beta(t) = \beta_0[1 + \beta_1 \cos(2\pi t/365)]$, generated annual epidemic cycles. Scenarios including disease-induced mortality demonstrated the impact of population decline on transmission dynamics.

1 Introduction

Infectious diseases pose a significant global health challenge, driven by the emergence of novel pathogens and the growing problem of antimicrobial resistance. Mathematical modeling provides essential tools for analyzing transmission dynamics, predicting outbreak trajectories, and evaluating the effectiveness of intervention strategies. Compartmental models, which classify individuals by disease status, have been particularly effective in informing public health responses to epidemics such as seasonal influenza and human immunodeficiency virus (HIV) [11].

The Susceptible-Infected-Recovered (SIR) model, introduced by Kermack and McKendrick in 1927, serves as a cornerstone of mathematical epidemiology. This model divides the population into three compartments: susceptible (S), infected (I), and recovered (R). Transitions between these compartments are governed by defined transmission and recovery rates. The model establishes that an epidemic can occur only if the basic reproduction number (R_0) exceeds one, assuming a completely susceptible population. Extensions that incorporate demographic changes, latent infection periods, and seasonal variations enable more accurate modeling of endemic diseases and epidemic cycles [11].

This report presents a computational analysis of the SIR model and its epidemiological extensions using numerical integration techniques. The study first calibrates the classical SIR model to data from a documented influenza outbreak in a boarding school to estimate transmission parameters. The analysis then incorporates demographic processes, such as births and deaths, as well as infection-induced mortality, and the Susceptible-Exposed-Infected-Recovered (SEIR) model, which includes a latent period. Seasonal transmission is modeled using sinusoidal variation, and the effectiveness of vaccination strategies, as described by Keeling et al. (2008), is assessed.

The numerical simulation experiments provide important epidemiological insights. Analysis of the boarding school outbreak estimates a basic reproduction number (R_0) of 3.72, corresponding to a critical vaccination threshold of 73.1 % for achieving herd immunity. Demographic model extensions reveal endemic equilibrium states characterized by damped oscillations with a period of approximately 2.4 years. The infection-induced mortality scenario demonstrates the impact of high fatality rates on population size. Seasonal variation analysis shows a shift to annual epidemic patterns as the amplitude of transmission increases. The following sections detail the theoretical background, computational methodology, results, and broader epidemiological significance.

2 Theory

This section presents the mathematical foundations of compartmental epidemic models. The exposition follows standard methodology, particularly that of Keeling and Rohani, and highlights the threshold structure governing epidemic invasion and persistence [11].

2.1 The Classical SIR Model

The standard Susceptible-Infected-Recovered (SIR) model divides a closed population into three mutually exclusive groups: susceptible individuals (S) who may acquire infection, infected individuals (I) who can transmit disease, and recovered individuals (R) who have lifelong immunity. Assuming homogeneous mixing, the model dynamics follow these equations.

$$\frac{dS}{dt} = -\beta SI \tag{1}$$
$$\frac{dI}{dt} = \beta SI - \gamma I \tag{2}$$
$$\frac{dR}{dt} = \gamma I \tag{3}$$

Here, β denotes the transmission rate, defined as the product of contacts per unit time and the probability of transmission per contact. The parameter γ represents the recovery rate, which is the inverse of the mean infectious period. The total population remains constant, such that $S(t) + I(t) + R(t) = N$ for all $t \geq 0$ [11, 9].

A key epidemiological insight of the SIR model is the definition of the basic reproduction number:

$$R_0 = \frac{\beta}{\gamma} \tag{4}$$

which represents the expected number of secondary infections produced by a single infectious individual in a completely susceptible population [11].

The threshold condition $R_0 > 1$ determines whether an epidemic can occur. When $R_0 \leq 1$, the infection declines exponentially. If $R_0 > 1$, the epidemic grows until the reduction of the susceptible population leads to the extinction of the outbreak [11].

The model has two equilibrium states. The disease-free equilibrium $(S^*, I^*, R^*) = (1, 0, 0)$ is globally stable when $R_0 \leq 1$. For $R_0 > 1$, trajectories converge to a post-epidemic equilibrium in which a fraction of the population has been infected. The final epidemic size is determined by the following transcendental equation.

$$R_\infty = 1 - S_0 \exp\left(-R_0 R_\infty\right) \tag{5}$$

where S_0 is the initial susceptible fraction and R_∞ represents the proportion of recovered individuals [11].

2.2 SIR Model with Demography

Demographic factors are important for modeling long-term diseases. The demographic SIR model includes constant per-capita birth and death rates (μ), which keep population stable and allow endemic equilibria. The following system of differential equations represents the model.

$$\frac{dS}{dt} = \mu - \beta SI - \mu S \tag{6}$$
$$\frac{dI}{dt} = \beta SI - (\gamma + \mu)I \tag{7}$$
$$\frac{dR}{dt} = \gamma I - \mu R \tag{8}$$

In this model, new births enter the susceptible compartment at rate μ, and all individuals are subject to natural mortality at the same rate. This structure ensures that the sum $S(t) + I(t) + R(t)$ remains equal to one for normalized populations [9, 11].

The basic reproduction number for the demographic SIR model is given by the following expression.

$$R_0 = \frac{\beta}{\gamma + \mu} \tag{9}$$

This value reflects the shorter infectious period from natural mortality. If R_0 is greater than one, the system reaches a unique endemic equilibrium.

$$(S^*, I^*, R^*) = \left(\frac{1}{R_0}, \frac{\mu(R_0 - 1)}{\beta}, 1 - S^* - I^*\right) \tag{10}$$

The endemic equilibrium features damped oscillations with period $T \approx 2\pi\sqrt{AG}$. Here, $A = 1/[\mu(R_0 - 1)]$ is the mean age at infection, and $G = 1/(\gamma + \mu)$ is the generation time [11].

2.3 SEIR Model

Some infectious diseases include an incubation period during which individuals are infected but not yet capable of transmitting the disease. The SEIR model incorporates this latent stage by introducing an exposed compartment, denoted as E, between the susceptible and infectious states.

$$\frac{dS}{dt} = \mu - \beta SI - \mu S \tag{11}$$
$$\frac{dE}{dt} = \beta SI - (\mu + \sigma)E \tag{12}$$
$$\frac{dI}{dt} = \sigma E - (\mu + \gamma)I \tag{13}$$
$$\frac{dR}{dt} = \gamma I - \mu R \tag{14}$$

In this context, σ represents the rate at which individuals progress from the exposed to the infectious compartment, resulting in a mean latent period of $1/\sigma$.

The basic reproduction number for the SEIR model is given by the following expression.

$$R_0 = \frac{\beta\sigma}{(\mu + \sigma)(\mu + \gamma)} \tag{15}$$

The inclusion of the latent stage increases the generation time. Consequently, the rate of epidemic growth is reduced, and oscillatory behavior around the endemic equilibrium is more pronounced compared to the basic SIR model. [11].

2.4 SIR Model with Infection-Induced Mortality

Infectious diseases with substantial fatality rates require explicit modeling of infection-induced mortality. Incorporating mortality results in temporal variation of the total population, as infectious individuals either die from the disease or recover. The model is formulated as follows:

$$\frac{dX}{dt} = \mu N - \frac{\beta XY}{N} - \mu X \tag{16}$$

$$\frac{dY}{dt} = \frac{\beta XY}{N} - \frac{\gamma + \mu}{1 - \rho} Y \tag{17}$$

$$\frac{dZ}{dt} = \gamma Y - \mu Z \tag{18}$$

where $X(t), Y(t), Z(t)$ denote the absolute numbers of susceptible, infectious, and recovered individuals, respectively, and $N(t) = X(t) + Y(t) + Z(t)$ is the time-varying population size. The standard incidence term $\beta XY/N$ corresponds to *frequency-dependent* transmission, which maintains a constant per-capita contact rate irrespective of population size. The parameter $\rho \in [0, 1)$ represents the probability that an infectious individual dies from the disease before recovery or natural death [11].

2.5 Seasonal Forcing in Transmission

Seasonal patterns in infectious diseases are influenced by factors such as school terms, climate variation, and behavioral changes [11]. These effects are modeled by introducing periodic variation in the transmission rate as follows:

$$\beta(t) = \beta_0 \left[1 + \beta_1 \cos\left(\frac{2\pi t}{365} \right) \right] \tag{19}$$

Here, β_0 denotes the mean transmission rate, $\beta_1 \in [0, 1)$ determines the amplitude of seasonal variation, and time t is expressed in days to correspond with the annual forcing period [11].

In SEIR models, seasonal forcing produces complex dynamics. The time-averaged basic reproduction number is given by:

$$\langle R_0 \rangle = \frac{\beta_0 \sigma}{(\mu + \sigma)(\mu + \gamma)} \tag{20}$$

The instantaneous reproduction number $R_0(t) = \langle R_0 \rangle [1 + \beta_1 \cos(2\pi t/365)]$ oscillates throughout the year. [11, 6].

3 Methods

This section describes the computational framework applied to analyze the epidemic models introduced in Section 2. The following subsections outline the numerical integration methods, parameter estimation procedures, experimental design, and analysis techniques employed to characterize model dynamics and evaluate intervention effectiveness.

3.1 Numerical Integration and Solver Configuration

All models were solved numerically using the Python library SciPy, specifically the `scipy.integrate.solve_ivp` function with adaptive time-stepping algorithms. For standard epidemic models, the Prince-Dormand Runge-Kutta method of order 4(5) (RK45) was employed. This method offers embedded error estimation and dense output, which are appropriate for smooth, non-stiff differential equations [5].

For long-term demographic simulations exhibiting damped oscillations over multi-decade periods, the LSODA integrator was utilized. LSODA automatically detects stiffness and transitions between the Adams and backward differentiation formula methods as required [13]. Relative and absolute error tolerances were set to 10^{-8} and 10^{-10}, respectively, to ensure sufficient accuracy for parameter estimation and oscillation analysis.

Time scales were chosen according to the model type. Epidemic simulations used daily resolution over 14-50 day periods, while demographic analyses employed yearly units over the span of 50-200 years. Finally, the seasonal forcing model operated on daily steps over 5-year periods to capture multi-annual cycles.

3.1.1 The Runge-Kutta Method

3.2 Parameter Estimation

Calibration of the closed-population susceptible-infectious-recovered (SIR) model to the 1978 British boarding-school influenza outbreak employed nonlinear least squares optimization [1]. The dataset comprises daily counts of infected students over 15 days in a school with a total enrollment of 763.

The closed-population SIR system for this experiment, defined by Equations 1-3, was initialized with 762 susceptible individuals, one infectious individual, and zero recovered individuals. The objective function minimized was the sum of squared residuals.

$$J(\beta, \gamma) = \sum_{k=0}^{14} [I_{\text{model}}(t_k; \beta, \gamma) - I_{\text{observed}}(t_k)]^2 \tag{21}$$

Here, $I_{\text{model}}(t_k; \beta, \gamma)$ denotes the numerically integrated infectious count at day t_k. The L-BFGS-B algorithm was used for optimization, subject to the constraints $\beta > 0$ and $\gamma > 0$ to ensure meaningful parameter estimates.

Model predictions were generated by integrating Equations (1)-(3) using the fitted parameters. This approach yielded estimates for the basic reproduction number, $R_0 = \beta/\gamma$, and the critical vaccination threshold, $p_c = 1 - 1/R_0$ [11].

3.3 Experimental Design

Model behavior was characterized across a range of parameter values using systematic parameter sweeps. The experimental design encompassed scenarios from sub-epidemic conditions, where $R_0 < 1$, to severe epidemics, where $R_0 > 5$.

For the classical SIR model, transmission rates were set to $\beta \in \{1, 2.5, 3\}$ and recovery rates to $\gamma \in \{0.5, 0.1, 1.5\}$, with units of year^{-1}. This configuration generated a 3×3 parameter grid, spanning R_0 values from 0.67 to 30.

The demographic SIR extension incorporated transmission rates $\beta \in \{1.5, 2.5, 3.5\}$, recovery rates $\gamma \in \{0.6, 1.2, 1.8\}$, and a fixed birth and death rate $\mu = 1/70$ year^{-1}, corresponding to a 70-year life expectancy. This parameterization produced R_0 values from 1.24 to 5.70. Oscillatory dynamics were identified using parameters representative of a measles epidemic, specifically $\beta = 1.4247$ day^{-1}, $\gamma = 0.1429$ day^{-1}, and $\mu = 0.00039$ day^{-1}, with initial condition The model was initialized with $(S_0, I_0, R_0) = (0.1, 0.0001, 1 - S_0 - I_0)$ resulting in $R_0 = 9.97$.

For the susceptible-exposed-infectious-recovered (SEIR) analysis, the recovery rate was fixed at $\gamma = 0.25$ and the birth and death rate at $\mu = 1/70$. Transmission rates $\beta \in \{1.5, 2.5, 3.5\}$ and progression rates $\sigma \in \{0.05, 0.15, 0.25\}$ were varied to assess the effects of the latent period. This model was initialized with $(S_0, E_0, I_0, R_0) = (0.95, 0.05, 0.05, 0)$. The seasonal forcing experiment employed baseline transmission rates $\beta_0 \in \{1.5, 2.5, 3.5\}$ and forcing amplitudes $\beta_1 \in \{0.0, 0.3, 0.6, 0.9\}$ to demonstrate the transition from annual to multi-annual

epidemic cycles. The seasonal model has simulated using the initial condition $(S_0, E_0, I_0, R_0) = (0.99, 0.0001, 0.0001, 1 - S0 - I0 - E0)$.

3.4 Dynamical Analysis Methods

Phase space analysis offers insights into the long-term, or steady-state, behavior of epidemiological systems that extend beyond time series visualization. This analysis applies methods from dynamical systems theory to characterize equilibrium states, stability properties, and the structure of solution trajectories.

3.4.1 Fixed Point Analysis and Linear Stability Theory

Fixed points represent equilibrium states in which all compartment populations remain constant. Mathematically, these points satisfy the following condition:

$$\mathbf{f}(\mathbf{x}^*) = \mathbf{0} \tag{22}$$

Here, $\mathbf{x}^* = (S^*, I^*, R^*)$ denotes the equilibrium state vector.

For each identified equilibrium, local stability is assessed by linearizing the system. The Jacobian matrix, evaluated at the fixed point, is defined as follows:

$$\mathbf{J}(\mathbf{x}^*) = \left.\frac{\partial \mathbf{f}}{\partial \mathbf{x}}\right|_{\mathbf{x}=\mathbf{x}^*} \tag{23}$$

Stability classification is based on the Hartman-Grobman Theorem, which establishes topological equivalence between nonlinear flows and their linearizations near hyperbolic fixed points [16]. The eigenvalues λ_i of $\mathbf{J}(\mathbf{x}^*)$ determine local stability. Equilibria are stable if $\mathrm{Re}(\lambda_i) < 0$ for all eigenvalues and unstable if any $\mathrm{Re}(\lambda_i) > 0$.

3.4.2 Phase Portrait Construction

Phase portraits depict epidemic dynamics by visualizing trajectories within reduced coordinate systems. Nullclines are essential for partitioning the phase space. These curves are defined at points where the derivatives of the system's variables are equal to zero. The intersection of nullclines identifies fixed points, while their geometric arrangement determines the global flow structure [16].

In epidemiological contexts, saddle points typically correspond to unstable disease-free states, while stable nodes or spirals represent endemic equilibria with monotonic or oscillatory convergence patterns [11].

3.4.3 Oscillation Analysis

Spectral analysis quantifies cyclical fluctuations in infection levels within the population. This method examines long-term data collected after the disease reaches endemic equilibrium. Discrete Fourier transforms (DFT) are employed to extract dominant frequencies from power spectral density distributions [8].

$$P(\omega) = \left| \int_0^T I(t) e^{-i\omega t} dt \right|^2 \tag{24}$$

Here, T denotes the integration period and $I(t)$ refers to the time series of the infected population. For numerical implementation, the discrete form is applied to sampled data points I_n over N time steps.

$$P(\omega_k) = \left| \sum_{n=0}^{N-1} I_n e^{-i2\pi kn/N} \right|^2 \tag{25}$$

Oscillation periods are determined from peak frequencies in the power spectrum and converted to epidemiologically relevant units, such as years. Dominant oscillation amplitudes are obtained from peak magnitudes in the frequency domain, providing measures of oscillation length relative to the mean endemic level [11, 14].

3.5 Vaccination Strategy Evaluation

This section analyzes two vaccination approaches: pediatric coverage and emergency mass vaccination. Both strategies are evaluated using parameters fitted to the 1978 boarding school outbreak to determine intervention requirements and expected outcomes.

3.5.1 Pre-exposure Pediatric Vaccination

Pre-exposure vaccination establishes population immunity before the onset of an epidemic by reducing the effective number of susceptible individuals. Vaccination coverage is represented by adjusting the initial susceptible fraction:

$$S_0^{\text{vax}} = S_0(1-p) \tag{26}$$

In this context, $p \in [0,1]$ denotes the vaccination coverage fraction, and $S_0 = 762/763$ specifies the initial susceptible proportion in the boarding school experiment.

The critical vaccination threshold for epidemic prevention is derived from the basic reproduction number. Epidemic growth occurs when $R_0 S_0^{\text{vax}} > 1$, so the minimum coverage required to prevent outbreaks is:

$$p_c = 1 - \frac{1}{R_0} \tag{27}$$

This represents the classical herd immunity threshold, above which the effective reproduction number falls below unity and epidemic invasion becomes impossible [11].

3.5.2 Emergency Mass Vaccination

Emergency vaccination is implemented as an intervention during ongoing epidemics. The process is modeled by removing susceptible individuals from the population at a constant rate u (individuals per day):

$$\frac{dS}{dt} = -\frac{\beta SI}{N} - u \tag{28}$$

$$\frac{dI}{dt} = \frac{\beta SI}{N} - \gamma I \tag{29}$$

$$\frac{dR}{dt} = \gamma I \tag{30}$$

$$\frac{dV}{dt} = u \tag{31}$$

where $V(t)$ tracks the cumulative vaccinated population and the total population remains constant: $S(t) + I(t) + R(t) + V(t) = N$ [11].

The effectiveness of each strategy is assessed by comparing the peak number of infected individuals in baseline and vaccinated scenarios. The vaccination rate u is varied from 10 to

200 individuals per day, reflecting the boarding school context, to determine the relationship between vaccination intensity and epidemic control.

Numerical integration of the modified susceptible-infectious-recovered (SIR) equations is used to evaluate both vaccination strategies. Identical baseline parameters ($\beta = 1.665$ day^{-1}, $\gamma = 0.448$ day^{-1}, $R_0 = 3.72$) are applied, as derived from the parameter estimation in Section 3.2.

4 Results and Discussion

Numerical results are presented following the models introduced in Sections 2–3. All interpretations are based on the threshold logic of R_0 (see (4), (9), (15)) and, where relevant, the herd-immunity relation $p_c = 1 - 1/R_0$.

4.1 Basic SIR Model Dynamics

The classical SIR model displays distinct behaviors depending on whether the basic reproduction number R_0 is above or below the epidemic threshold of 1. Figure 1 illustrates this contrast using two representative cases: sub-epidemic dynamics at (a) $R_0 = 0.67$ and (b) epidemic dynamics at $R_0 = 5.00$.

In the sub-epidemic scenario ($R_0 = 0.67$ with $\beta = 1.0$, $\gamma = 1.5$), the susceptible population remains nearly constant at $S \approx 0.99$. This outcome confirms that when transmission is insufficient to offset recovery, $R_0 \leq 1$ prevents epidemic growth under all initial conditions.

Conversely, the epidemic scenario ($R_0 = 5.00$ with $\beta = 2.5$, $\gamma = 0.5$) generates a classical infection curve, with peak infection occurring at day 2. The final epidemic size approaches 100% of the population, in close agreement with the theoretical prediction from the transcendental relationship in equation (5).

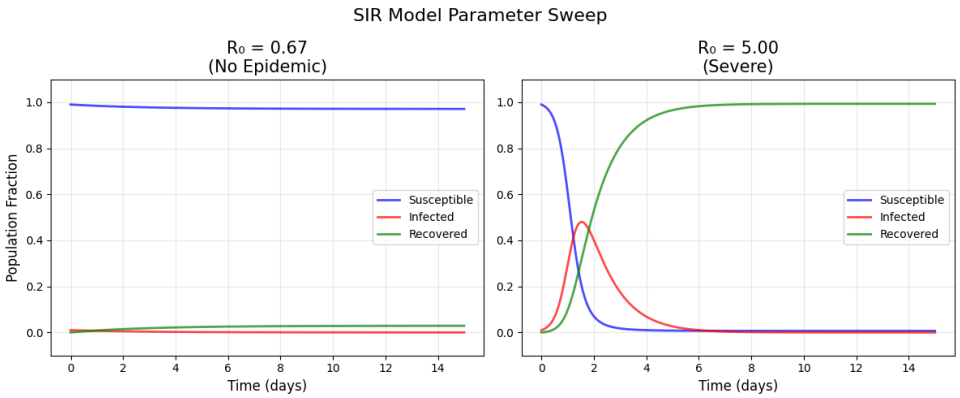

Figure 1: SIR model simulations comparing sub-epidemic and epidemic regimes. Graph (a) with $R_0 = 0.67$ ($\beta = 1.0$, $\gamma = 1.5$) shows infection failing to spread, with $S(t)$ nearly constant. Graph (b) with $R_0 = 5.00$ ($\beta = 2.5$, $\gamma = 0.5$) shows the epidemic curve peaking at day 2 and infecting nearly the entire population.

The phase space portraits in Figure 2 illustrate the geometric basis of these dynamics. The critical threshold $S = 1/R_0$ (indicated by the purple dashed line at $S = 0.20$ for $R_0 = 5.00$) divides the phase plane into regions of epidemic growth and decline. Sub-epidemic trajectories (a) move monotonically toward the disease-free state, whereas epidemic trajectories (b) reach peak infection before declining to post-epidemic equilibria along the $I = 0$ boundary.

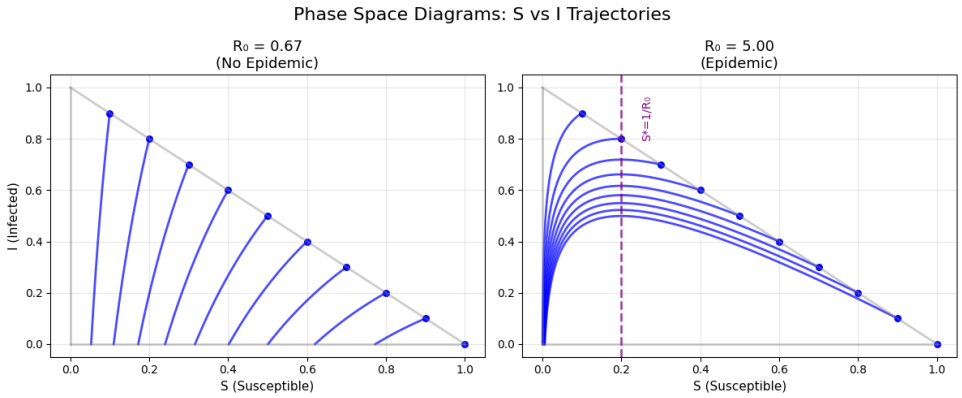

Figure 2: Phase space portraits of the SIR model. Graph (a) with $R_0 = 0.67$ shows monotonic decline toward the disease-free state. Graph (b) with $R_0 = 5.00$ shows epidemic growth before convergence to $I = 0$. The dashed purple line marks the threshold $S = 1/R_0$, separating invasion from decay.

4.2 Parameter Estimation from Historical Data

The SIR model was applied to the 1978 British boarding school influenza outbreak using nonlinear least squares optimization. The L-BFGS-B algorithm converged to fitted parameters $\beta = 1.665$ day^{-1} and $\gamma = 0.448$ day^{-1}, yielding a basic reproduction number $R_0 = 3.72$.

Figure 3 shows that model predictions closely align with observed data. The fitted curve accurately represents the exponential growth phase from days 0 to 6 and the subsequent decline, with the peak infection observed on day 6. Minor deviations in the later stages may result from stochastic effects or behavioral changes that are not accounted for in the deterministic model [11].

The estimated parameters define a critical vaccination threshold of $p_c = 1 - 1/R_0 = 73.1\%$ required for herd immunity. This threshold serves as a benchmark for the vaccination strategy analysis presented in Section 4.3.

4.3 Vaccination Strategy Evaluation

Fitted parameters from the boarding school outbreak ($\beta = 1.665$ day^{-1}, $\gamma = 0.448$ day^{-1}, $R_0 = 3.72$) were used to evaluate two vaccination approaches: pre-exposure pediatric coverage and emergency mass vaccination during active outbreaks.

4.3.1 Pre-exposure Vaccination

Figure 4 (a) illustrates the threshold effect across coverage levels ranging from 0 to 90 percent. In the absence of vaccination ($p = 0\%$, $R_{eff} = 3.69$), the outbreak results in a severe epidemic with a peak of 286 infections. Moderate coverage levels yield proportional reductions: 40 percent coverage reduces peak infections to approximately 130 individuals, and 60 percent coverage further limits peak prevalence to about 50 cases. Transmission continues until coverage nears the critical threshold.

The threshold effect is observed at $p = 73.1\%$, where the effective reproduction number reaches unity ($R_{eff} = 1.00$). Coverage exceeding this threshold prevents sustained transmission; 80 % and 90 % coverage reduce infections to sporadic cases.

4.3.2 Emergency Mass Vaccination

Emergency mass vaccination during outbreaks demonstrates a direct dose-response relationship between vaccination rate and epidemic severity. Figure 4 (b) presents the effects of daily

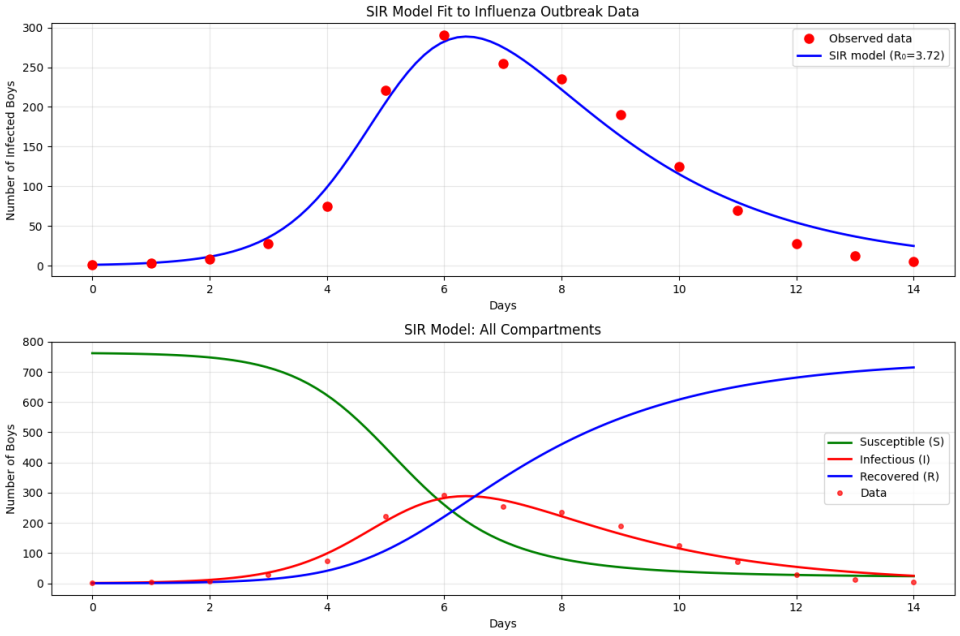

Figure 3: SIR model calibrated to the 1978 British boarding school influenza outbreak. Observed cases (dots) are compared with the fitted curve (line) obtained via nonlinear least squares (L-BFGS-B), using $\beta = 1.665$ day^{-1} and $\gamma = 0.448$ day^{-1} ($R_0 = 3.72$). The model reproduces the exponential rise to a peak on day 6 and the subsequent decline, with minor deviations in later stages.

vaccination rates ranging from 0 to 200 individuals on a single outbreak experiment.

Moderate vaccination rates of 25 to 50 individuals per day result in partial epidemic control, reducing peak infections from 286 to approximately 100 to 190 cases. Higher vaccination rates provide substantial mitigation, with 100 vaccinations per day lowering the peak prevalence to approximately 50 cases. The highest rate of 200 vaccinations per day nearly prevents the epidemic entirely and significantly reduces the outbreak duration.

4.4 SIR Model with Demographic Processes

Incorporating demographic processes enables endemic persistence and oscillatory behavior, thereby fundamentally altering the dynamics of the susceptible-infected-recovered (SIR) model. This effect is demonstrated using a simulation with a basic reproduction number $R_0 = 5.70$ over a 200-year period and a birth and death rate of $\mu = 1/70$ year^{-1}.

Figure 5 presents the system behavior. The scenario with $R_0 = 5.70$ exhibits damped oscillations that converge toward an endemic equilibrium.

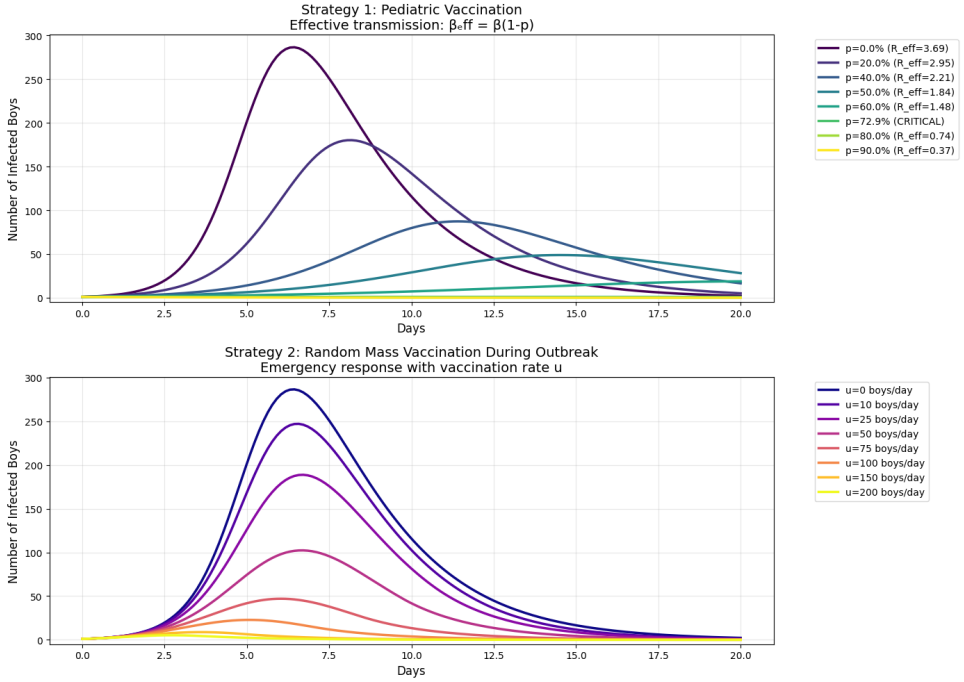

Figure 4: Vaccination strategies simulated with fitted parameters from the 1978 British boarding school outbreak ($R_0 = 3.72$). Graph (a) shows pre-exposure pediatric vaccination, where epidemic size declines sharply once coverage exceeds the herd immunity threshold ($p_c = 73.1\%$). Graph (b) shows emergency mass vaccination during an outbreak; higher daily vaccination rates progressively reduce peak infections and outbreak duration.

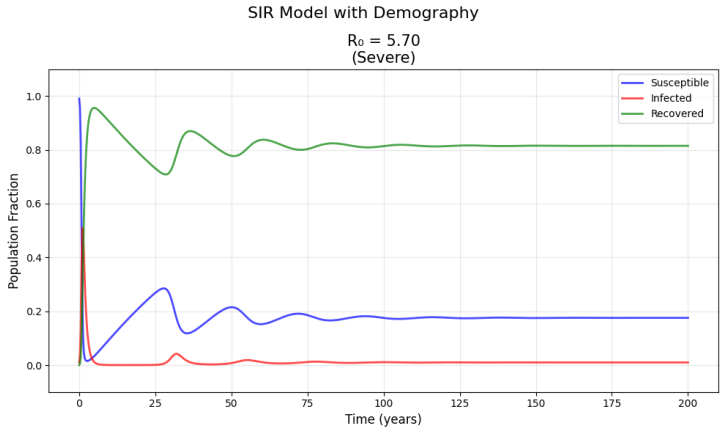

Figure 5: SIR model with demography ($\mu = 1/70$ year^{-1}) at $R_0 = 5.70$. The system exhibits damped oscillations that converge to a stable endemic equilibrium.

The phase space portrait in Figure 6 highlights the geometric structure underlying these dynamics. The graph demonstrates spiraling convergence toward the endemic equilibrium, indicated by the red point. This spiral pattern illustrates the interaction between epidemic dynamics and demographic renewal, as births continuously update the susceptible population and maintain transmission cycles [16].

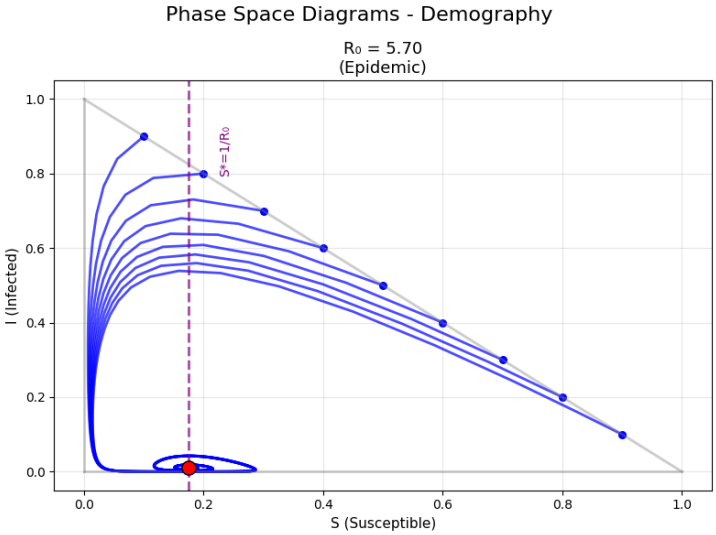

Figure 6: The phase space portrait of the susceptible-infectious-recovered (SIR) model with demographic turnover, where the basic reproduction number (R_0) is 5.70, demonstrates that trajectories spiral inward toward the endemic equilibrium, indicated by the red point. This pattern reflects damped oscillations resulting from the continuous introduction of susceptible individuals through births.

4.4.1 Damped Oscillatory Dynamics

The parameters $\beta = 1.4247$ day^{-1}, $\gamma = 0.1429$ day^{-1}, and $\mu = 0.00039$ day^{-1} were selected to generate pronounced oscillatory dynamics, resulting in a basic reproduction number $R_0 = 9.97$. The model was integrated over a 80-year period using initial conditions that were slightly perturbed from the theoretical equilibrium values $S^* = 0.1003$, $I^* = 0.000246$, and $R^* = 0.8995$.

Figure 7 illustrates damped oscillations in the infected and susceptible compartments. The susceptible population (a) oscillates around the theoretical equilibrium $S^* = 1/R0 = 0.1003$ with a progressively decreasing amplitude.

The infected population (b) exhibits similar oscillations around the endemic equilibrium $I^* = 0.000246$. Frequency analysis reveals a dominant oscillation period of 2.40 years, consistent with the theoretical prediction $T \approx 2\pi\sqrt{AG}$ where $A = 1/[\mu(R_0 - 1)]$ represents the mean age at infection and $G = 1/(\gamma + \mu)$ is the generation time. The observed cyclic pattern gradually converges to steady-state endemic levels.

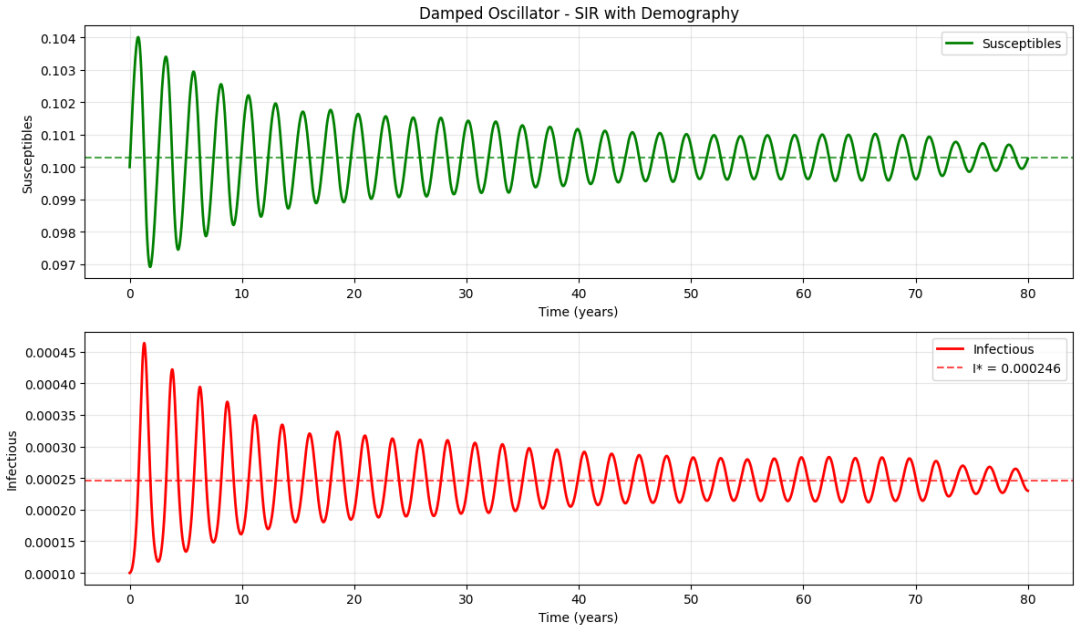

Figure 7: Damped oscillations in the demographic SIR model with $R_0 = 9.97$ ($\beta = 1.4247$, $\gamma = 0.1429$, $\mu = 0.00039$ day^{-1}). Graph (a) shows the susceptible fraction oscillating around the equilibrium $S^* = 1/R_0 = 0.1003$, while graph (b) shows the infected fraction oscillating around $I^* = 0.000246$. Both exhibit decreasing amplitude with a dominant period of 2.40 years, converging to endemic equilibrium.

4.5 Infection Induced Mortality

Incorporating infection-induced mortality enables the population size to change dynamically throughout the simulation period. The analysis examined mortality probabilities (ρ) from 0 to 0.8, applying baseline parameters of transmission rate ($\beta = 2.5$ year^{-1}), recovery rate ($\gamma = 0.5$ year^{-1}), and natural mortality rate ($\mu = 1/70$ year^{-1}) over a 50-year integration.

Figure 8 presents the effects of increasing mortality rates from three analytical perspectives. Graph (a) depicts the total population size over time. In the absence of infection-induced mortality ($\rho = 0.0$, blue line), the population remains stable. At moderate mortality ($\rho = 0.4$, yellow line), the population decreases to approximately 60 percent of its initial size. Elevated mortality probabilities ($\rho = 0.6$ and 0.8) cause major population declines. High mortality ($\rho = 0.8$, purple line) results in rapid population decline.

Graph (b) demonstrates the impact of mortality on infection dynamics. Higher mortality rates, lower peak infection levels, and delayed epidemic peaks. The baseline scenario ($\rho = 0.0$) yields a sharp epidemic peak at approximately 45 % infection. Increasing mortality reduces the infected fraction: $\rho = 0.4$ limits peak infection to about 30 percent, and $\rho = 0.8$ reduces it to approximately 20 percent. This outcome reflects the dual effect of mortality, which increases per-capita death rates and reduces the effective population available for transmission.

The compartment analysis for $\rho = 0.4$ (c) illustrates modified dynamics under specific mortality scenario. The total population (black dashed line) declines from unity to approximately 60 percent. The susceptible population (blue) decreases during the epidemic and gradually recovers as births replenish the population. The infected compartment (red) displays a typical epidemic curve with reduced magnitude. The recovered population (green) increases and then gradually declines due to natural mortality.

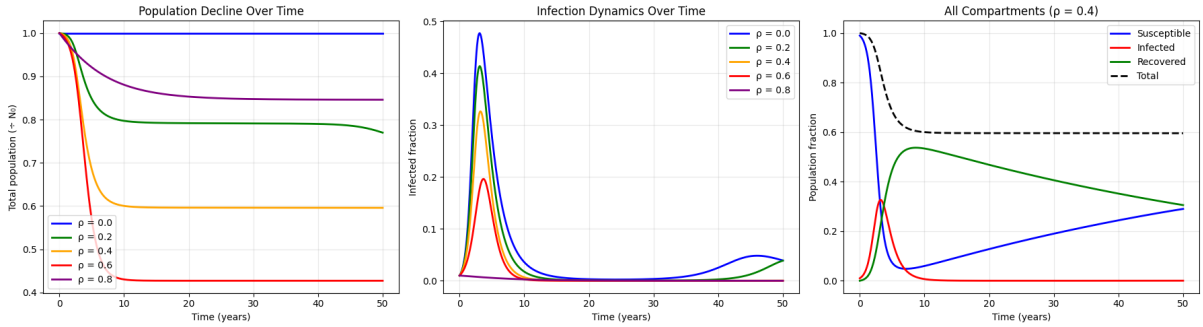

Figure 8: Effects of infection-induced mortality on demographic SIR dynamics, using parameters $\beta = 2.5$ yr^{-1}, $\gamma = 0.5$ yr^{-1}, and $\mu = 1/70$ yr^{-1}. In graph (a), population size declines over time as mortality probability ρ increases from 0.0 to 0.8, which leads to a faster population decrease. Graph (b) presents infection trends, showing that higher ρ values result in lower and later epidemic peaks. Graph (c) illustrates compartment trajectories for $\rho = 0.4$, with reduced population size, lower infection peak, and recovery through births.

4.6 SEIR Model

The SEIR model incorporates a latent period between infection and infectiousness, which changes epidemic dynamics by introducing an exposed compartment. The key differences from the basic susceptible-infectious-recovered (SIR) framework are illustrated using a representative case with $R_0 = 4.41$.

Figure 9 presents the dynamics of all four compartments throughout the simulation period. The exposed population (yellow) accumulates rapidly as susceptible individuals transition to the exposed state before becoming infectious. This compartment peaks during the initial epidemic phase and declines to low endemic levels.

The infected compartment (red) exhibits delayed epidemic progression relative to equivalent SIR scenarios, as peak infectiousness is influenced by the presence of the latent stage.

The susceptible compartment (blue) exhibits expected depletion and ultimately converges to the theoretical equilibrium. The adjusted basic reproduction number $R_0 = \beta\sigma/[(\mu+\sigma)(\mu+\gamma)]$ quantifies the reduction in transmission efficiency resulting from the latent period.

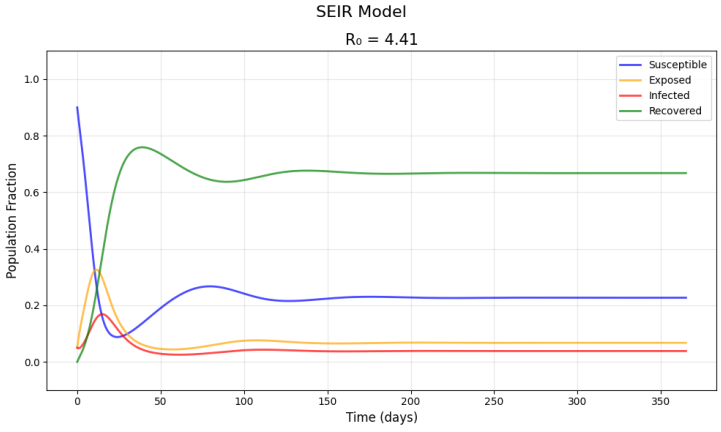

Figure 9: SEIR model dynamics with $R_0 = 4.41$. The exposed compartment (yellow) rises sharply before declining to low endemic levels, delaying the epidemic peak in the infected compartment (red) relative to SIR dynamics. The susceptible population (blue) follows expected decline toward equilibrium, while the recovered population (green) accumulates over time.

Phase space analysis reveals the geometric impact of the latent period on the dynamics of

epidemics. Figure 10 compares trajectory flows for (a) SEIR and (b) SIR models with identical parameters ($R_0 = 4.41$).

Both models converge to the same endemic equilibrium at $S^* = 1/R_0 \approx 0.227$, which confirms that threshold behavior and steady states are preserved. However, the trajectory geometries differ significantly. SEIR model trajectories (a) display gradual, curved approaches that reflect the effect of the exposed compartment. In contrast, SIR model trajectories (b) demonstrate more direct convergence patterns resulting from immediate transitions from susceptible to infectious states.

This comparison indicates that although threshold criteria and endemic outcomes are identical, the inclusion of a latent period fundamentally influences epidemic timing and trajectory shapes. The SEIR model therefore provides a more realistic representation of diseases characterized by incubation periods.

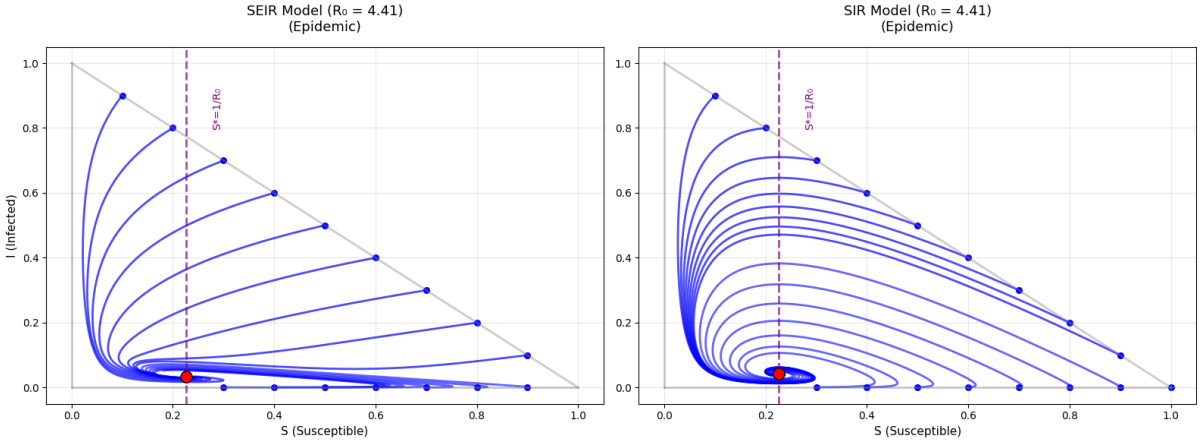

Figure 10: Phase space comparison of SEIR and SIR models with $R_0 = 4.41$. Graph (a) shows SEIR trajectories converging toward the endemic equilibrium ($S^* = 1/R_0 \approx 0.227$), reflecting the effect of the exposed compartment. Graph (b) shows SIR trajectories converging more directly, as infections occur immediately after exposure.

4.7 Seasonal Effects in SEIR Model

Incorporating seasonal forcing into the susceptible-exposed-infectious-recovered (SEIR) model produces transitions within annual epidemic dynamics. Seasonal variation in transmission is represented by sinusoidal modulation: $\beta(t) = \beta_0(1 + \beta_1 \cos(2\pi t))$, where β_1 is the amplitude of seasonal forcing and t is time in years.

Figure 11 illustrates the shift from equilibrium dynamics to complex periodic behavior as the seasonal forcing amplitude β_1 increases from 0.0 to 0.9. The fixed parameters result in a basic reproduction number $R_0 = 4.44$, which maintains endemic conditions and isolates the effects of seasonal forcing.

For $\beta_1 = 0.0$, the system exhibits a stable endemic equilibrium with constant population fractions. The addition of weak seasonal forcing ($\beta_1 = 0.3$) generates annual epidemic cycles synchronized with the seasonal transmission pattern. Moderate forcing amplitude ($\beta_1 = 0.6$) produces large-amplitude annual epidemics. The susceptible population exhibits corresponding decrease during outbreaks, which reflects the buffered transmission that occurs during favorable seasonal conditions. Strong seasonal forcing ($\beta_1 = 0.9$) amplifies these annual dynamics to extreme levels.

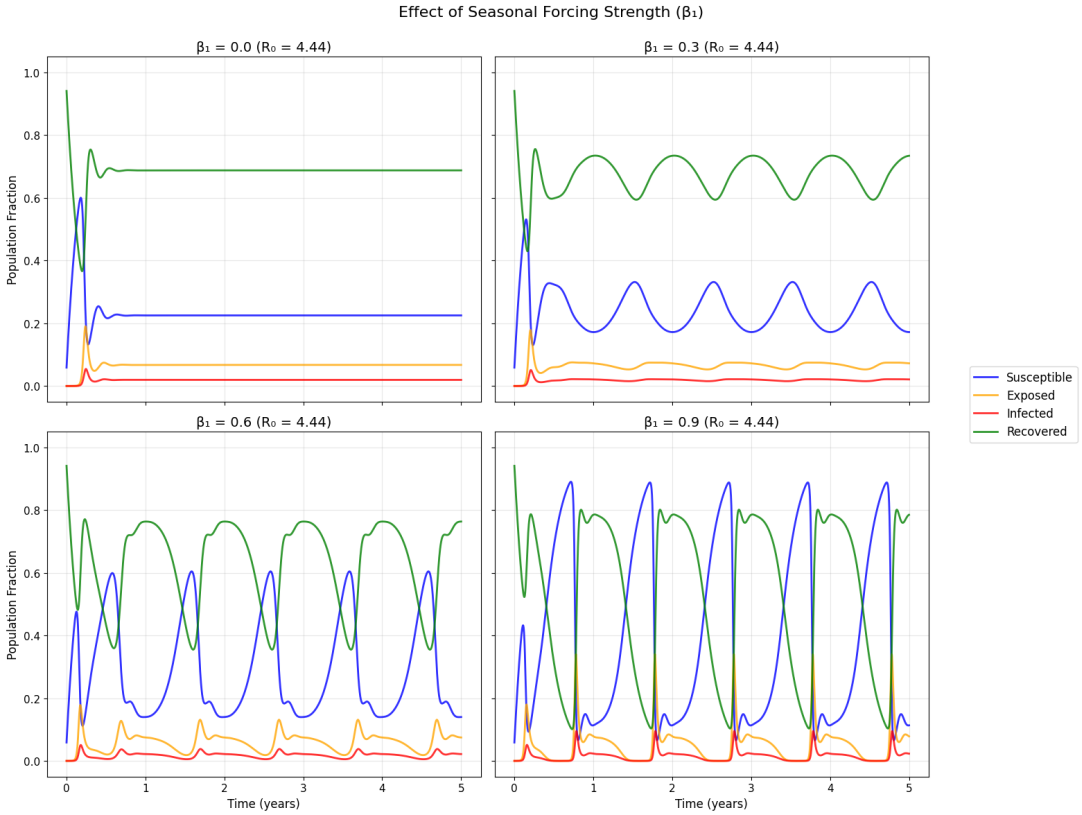

Figure 11: SEIR model with seasonal forcing ($R_0 = 4.44$). Increasing the forcing amplitude β_1 shifts dynamics from a stable endemic equilibrium ($\beta_1 = 0.0$) to annual epidemic cycles ($\beta_1 = 0.3$), large-amplitude annual outbreaks ($\beta_1 = 0.6$), and extreme seasonal epidemics ($\beta_1 = 0.9$).

5 Conclusions

Analysis of susceptible-infectious-recovered (SIR) epidemiological models reveals that the basic reproduction number R_0 is the primary determinant of epidemic dynamics across model variations, under the assumption of a completely susceptible population. Estimation of parameters from the 1978 boarding school influenza outbreak established a critical vaccination threshold and demonstrated the effectiveness of two standard control strategies.

Incorporating demographic processes, such as birth and death, explained the mechanisms underlying endemic persistence. Experiments on infection-induced mortality clarified the relationship between disease severity and transmission dynamics, indicating that higher fatality rates may reduce epidemic spread by depleting the population.

Extending the model to include a susceptible-exposed-infectious-recovered (SEIR) structure demonstrated that latent periods delay epidemic peaks without altering threshold criteria. Analysis of seasonal forcing revealed transitions within annual epidemic cycles. These results indicate that environmental conditions can generate complex temporal patterns [6, 7].

The threshold structure of R_0 offers a robust framework for interpreting epidemic invasion, persistence, and control across diverse biological and demographic contexts. The results indicate that compartmental epidemic models can capture essential features of infectious disease dynamics and provide a computational basis for vaccination policy development and epidemic preparedness.[11, 9].

References

[1] Avilov, K. K., Li, Q., Lin, L., Demirhan, H., Stone, L., & He, D. (2024). The 1978 English boarding school influenza outbreak: where the classic SEIR model fails. *Journal of the Royal Society Interface*, 21(213), 20240394.

[2] Byrd, R. H., Lu, P., Nocedal, J., & Zhu, C. (1995). A limited memory algorithm for bound constrained optimization. *SIAM Journal on Scientific Computing*, 16(5), 1190-1208.

[3] Cantó, B., Coll, C., & Sánchez, E. (2017). Estimation of parameters in a structured SIR model. *Advances in Difference Equations*, 2017, 33.

[4] Church, D. L. (2004). Major factors affecting the emergence and re-emergence of infectious diseases. *Clinical Laboratory Medicine*, 24(3), 559-586.

[5] Dormand, J. R., & Prince, P. J. (1980). A family of embedded Runge-Kutta formulae. *Journal of Computational and Applied Mathematics*, 6(1), 19-26.

[6] Earn, D. J., Rohani, P., Bolker, B. M., & Grenfell, B. T. (2000). A simple model for complex dynamical transitions in epidemics. *Science*, 287(5453), 667-670.

[7] Grassly, N. C., & Fraser, C. (2006). Seasonal infectious disease epidemiology. *Proceedings of the Royal Society B: Biological Sciences*, 273(1600), 2541-2550.

[8] Heinzel, G., Rüdiger, A., & Schilling, R. (2002). Spectrum and spectral density estimation by the Discrete Fourier transform (DFT), including a comprehensive list of window functions and some new flat-top windows. Max-Planck-Institut für Gravitationsphysik (Albert-Einstein-Institut), Teilinstitut Hannover.

[9] Hethcote, H. W. (2000). The mathematics of infectious diseases. *SIAM Review*, 42(4), 599-653.

[10] Keeling, M. J., Rohani, P., & Grenfell, B. T. (2001). Seasonally forced disease dynamics explored as switching between attractors. *Physica D: Nonlinear Phenomena*, 148(3-4), 317-335.

[11] Keeling, M. J., & Rohani, P. (2008). *Modeling infectious diseases in humans and animals*. Princeton University Press.

[12] Kermack, W. O., & McKendrick, A. G. (1927). A contribution to the mathematical theory of epidemics. *Proceedings of the Royal Society of London. Series A*, 115(772), 700-721.

[13] Petzold, L. (1983). Automatic selection of methods for solving stiff and nonstiff systems of ordinary differential equations. *SIAM Journal on Scientific and Statistical Computing*, 4(1), 136-148.

[14] Press, W. H., Teukolsky, S. A., Vetterling, W. T., & Flannery, B. P. (2007). *Numerical Recipes: The Art of Scientific Computing* (3rd ed.). Cambridge University Press.

[15] Soper, H. E. (1929). The interpretation of periodicity in disease prevalence. *Journal of the Royal Statistical Society*, 92(1), 34-73.

[16] Strogatz, S. H. (2015). *Nonlinear Dynamics and Chaos: With Applications to Physics, Biology, Chemistry, and Engineering*. CRC Press.